Observed changes in the Arctic Freshwater Outflow in Fram Strait

T. Karpouzoglou[1,2], L. de Steur[1], L.H. Smedsrud[2], and H. Sumata[1]

[1]Norwegian Polar Institute, Tromso, Norway
[2]Geophysical Institute, University of Bergen, Bergen, Norway

Key Points:

- The freshwater transport of the East Greenland Current in the Fram Strait decreased due to lower volume transport and freshwater content.
- The salinity stratification within Polar Water increase while the Polar Water depth and the eastward extent of the Polar layer decrease.
- Novel data have improved the seasonality of the freshwater transport and have decreased the uncertainty.

Corresponding author: T.Karpouzoglou, `thodoris.karpouzoglou@npolar.no`

Abstract

We present year-round estimates of liquid freshwater transport (FWT) in the East Greenland Current (EGC) in the western Fram Strait from mooring observations since 2015. Novel data from additional instruments deployed in recent years are used to correct earlier estimates when instrument coverage was lower. The updated FWT time series (reference salinity 34.9) show that the increased export between 2010 and 2015 has not continued, and that FWT has decreased to pre-2009 levels. Salt transport independent of a reference salinity is shown not to be sensitive to salinity changes. Between 2015-2019, the FWT in the Polar Water decreased to an average of 56.9 ($\pm$4.5) mSV, 15% less than the 2003-2019 long-term mean, however, high FWT events occurred in 2017. The overall decrease is related with a slowdown of the EGC, partly attributed to a decrease of the baroclinic component, due to salinification of the halocline waters ($26.5 < \sigma_\theta < 27.7\ kg/m^3$) which counterbalanced the freshening of the surface layer ($\sigma_\theta < 26.5\ kg/m^3$). Our results show changes in the Polar Water between 2003-2019: Salinity stratification increases as the salinity difference between 155 and 55 m increased by 0.63 psu , the Polar Water layer became thinner by 46 m and the Polar-Atlantic front moved abruptly west in June 2015. All processes point to an "Atlantification" of the western Fram Strait and reduced Polar outflow. Including the novel data sets decreased the uncertainty of the FWT to an average of 8% after 2015, as opposed to 17% in earlier estimates.

Plain Language Summary

The East Greenland Current brings fresh and cold Polar Water southwards from the Central Arctic Ocean. In the Fram Strait, between Greenland and Svalbard, the strength and properties of this current has been observed using current meters and temperature and salinity sensors since 1997. We present updated data for the 2015-2019 period and re-analyse earlier variability and estimates. The earlier estimates of freshwater transport are evaluated based on an improved set of observations and found to be of good accuracy. The main finding is that the freshwater transport since 2015 has decreased. This decrease is caused by a reduction in the southward flow speed and amount of the fresh Polar Water. The front between Polar and Atlantic water has moved westward, and the Polar Water layer has become thinner and more stratified. We also refine the seasonal variability of the East Greenland current based on the new data, discuss how freshwater transport values depend on the chosen reference salinity, and possible connections towards Arctic freshwater storage.

1 Introduction

The Arctic is experiencing rapid changes related to anthropogenic climate change (Jahn & Laiho, 2020; Haine, 2020). Arctic warming and rising air-temperature leads to a more intense hydrological cycle, and rapid ice retreat, leading to increased liquid freshwater input to the Arctic Ocean (Collins et al., 2013; Graham et al., 2017; Shu et al., 2018). Freshwater (both liquid and and sea-ice) circulate in the central Arctic Ocean with the surface currents and exit through the Fram Strait and the Canadian Archipelago. Freshwater anomalies entering the Nordic Seas and Subpolar North Atlantic may modify dense water formation and therefore the strength of the Atlantic Meridional Overturning Circulation (AMOC) (Stommel, 1961; Heuzé, 2017; Le Bras et al., 2021). So far, however, measurements of the AMOC reveal strong variability and the current length of the time series has been shown to be too short in order to identify a significant trend (Lobelle et al., 2020). Motivated by the observed rapid increase of the freshwater storage in the Arctic in the 2000s (McPhee et al., 2009; Proshutinsky et al., 2009; Rabe et al., 2014; Proshutinsky et al., 2019), and the projected freshening by the end of the century (Collins et al., 2013; Lique et al., 2016; Shu et al., 2018; Jahn & Laiho, 2020), we analyse the Arctic freshwater outflow through the Fram Strait, as it reflects changes occurring in the central Arctic Ocean and alerts for potential future ones in the Nordic Seas and the Subpolar North Atlantic.

The Fram Strait lies between North-east Greenland and the Svalbard archipelago (Figure 1a) and is the largest and deepest gateway between the central Arctic Ocean and the Nordic Seas. The deep part of the strait has a maximum depth of around 2600 m and steep slopes connect it to the much shallower continental shelves of Greenland and Svalbard. Following the continental slope in the western side of the strait, cold and fresh Polar Water (PW) and sea-ice are exported from the Arctic with the East Greenland Current (EGC) (Aagaard & Carmack, 1968a). Along the continental slope to the east, the West Spitsbergen Current (WSC) brings warm Atlantic water (AW) to the central Arctic Ocean (Mosby, 1962), while branches of AW recirculate within the Fram Strait and flow southward alongside the PW (Quadfasel et al., 1987). The EGC carries about half of the liquid freshwater export of the Arctic Ocean and nearly 90% of the sea-ice (see references in Haine et al. (2015)). Despite the challenging field conditions in the western Fram Strait, a large and up-to-date dataset has emerged from the ocean moorings of the Fram Strait Arctic Outflow Observatory (FSAOO), providing hydrographic and current data from the EGC at 78°50'N since 2002 (79°N before that) allowing the study of the year-round Arctic freshwater outflow (De Steur et al., 2018).

Freshwater content in the ocean is defined as the amount of zero-salinity water required to reach an observed salinity, starting from a chosen reference value (Haine et al., 2015). One of the first indications of an increasing freshwater content in the Arctic Ocean came by Proshutinsky et al. (2009), who reported an increase of the freshwater content in the Beaufort Gyre between 2003-2007. Rabe et al. (2014), using both observations and model data reported a rapid Arctic-wide increase of the freshwater content between 2000 and 2009. This increase, identified by the literature, was accompanied by an intensification of the Beaufort Gyre leading to convergence of freshwater in the area (Proshutinsky et al., 2009; Giles et al., 2012; Rabe et al., 2014) and possibly to a reduction of the Arctic freshwater outflow. In accordance with that, De Steur et al. (2009) identified a decrease in freshwater outflow through the Fram Strait between 2005 and 2009, while other studies reported no significant changes (Rabe et al., 2013; Marnela et al., 2016). Between 2009 and 2015 the spin-up of the Beaufort Gyre and the freshening of the Canadian Basin equilibrated (Zhang et al., 2016), but since 2016 the freshening continued (Proshutinsky et al., 2019). The last record of the observed liquid freshwater outflow through Fram Strait showed a period of increased freshwater transport between 2010 and 2015, concurring with the equilibration of the Beaufort Gyre, and accumulating to a significant freshwater volume anomaly (De Steur et al., 2018). After 2015, the freshwater transport in the Fram Strait is unknown, and it is unclear if the freshwater transport continued to increase, or if it had decreased, possibly in response to an intensifying Beaufort gyre.

In this paper, we present updated freshwater transport estimates through the western Fram Strait based on year-round ocean mooring records collected by the FSAOO between 2015-2019. Moreover, we correct estimates from the previous years, which had fewer instruments, to make a consistent time series allowing for comparison. We show that the large increase in freshwater transport observed by De Steur et al. (2018) did not continue after 2015, however, interannual variability has been large. We present the total volume transport and freshwater content through the full depth mooring array as well as for the Polar Water only, and describe changes in hydrography and current properties between 2003 and 2019. To address concerns related to the dependence of freshwater transport on a reference salinity (Schauer & Losch, 2019), we additionally provide salt transport values, as salt transport is independent of a reference value, and discuss the strengths and limitations of the two variables. Finally, we calculate the uncertainty of freshwater transport, and show how this has decreased over time with increasing instrument coverage.

2 Material and Methods

2.1 Mooring data

Since 1997 and up to present, high-frequency year-round hydrographic data have been collected by the FSAOO across the East Greenland Current, between 0.3°W and 8°W longitude (De Steur et al., 2014). Between September 2015 and August 2016, the year of maximum instrument coverage, the array consisted of eight moorings: F9, F10, F11, F12, F13, F13b, F14, and F17 positioned at: 0.75°W, 2°W, 3°W, 4°W, 5°W, 5.5°W, 6.5°W, and 8°W longitude, respectively (Figure 1b). Moorings F11 up to F17 have been maintained by the Norwegian Polar Institute since 1997 (more details given below). Moorings F9 and F10 have been operated by the Alfred Wegener Institute until September 2016. Since then, F9 has been discontinued and since 2017, the Norwegian Polar Institute has continued F10. The composition of FSAOO has changed significantly over the years (Figure 2). This, since more moorings, instruments and technologies have been implemented, increasing the spatial coverage of the array. In addition, however, there have also been periods with significant data gaps due to lost moorings (De Steur et al., 2014; De Steur et al., 2018).

A prominent improvement in the composition of FSAOO took place in September 2003 when mooring F17 was added at 8°W resulting in a clear increase of the captured southward freshwater transport (FWT) (De Steur et al., 2018). As of September 2015, mooring F13b was added over the continental slope. Overall, the number of sampling points of the FSAOO has increased significantly in recent years providing better coverage of the EGC (Figure 2). This study focuses on the moorings F10 through F17 between September 2003 and September 2019. Mooring F9 which has not been operated since September 2016, is excluded from this analysis.

Since most of the FWT occurs in the upper water column, near-surface salinity and velocity measurements are essential. However, the acquisition of year-round salinity data in the top 50 m of the water column has been challenging due to the presence of icebergs and deep-reaching sea-ice keels that, until recently, did not allow the deployment of instruments near the surface. Since 2013, Inductive Modem (IM) SBE37 Microcats (so called IceCATs) have been installed with a weak link (Curry et al., 2014) at 25 m target depth. However, until September 2019, the year-round IceCAT data are limited to four successful deployments (F13b: 2013, 2014, F17: 2015, 2017). Another significant addition to the instrumentation of FSAOO was the deployment of extra SBE37 sensors between 70 and 170 m depth, at moorings F12 to F14 (F12: 2016, 2018, F13: 2013 to 2018, F13b: 2014 to 2018, F14: 2016, 2018), that reduced interpolation errors between instruments at $\sim$ 55 m and 250 m depth. Apart from those, the array contains a combination of Seabird sensors (SBE 16, 37) measuring conductivity, temperature and depth, of Recording Current Meters (RCM 7, 8, 9, 11) with additional sensors measuring horizontal velocities, temperature and depth, and of Aanderaa Doppler Current Meter (DCM12), Aanderaa Recording Doppler Current Meter (RDCP600), or RDI Acoustic Doppler Current Profilers (ADCP) installed at $\sim$ 55 m providing velocity profiles between 50 m and 10 m below the surface. In general, the sampling intervals of salinity, velocity, temperature and pressure vary between 15 min to 2 h (De Steur et al., 2014).

2.2 CTD data

Since the first deployment of the mooring array, a CTD section is repeated every August/September during the annual maintenance of the array. In addition, five CTD sections from cruises crossing the Fram Strait during April/May are available (2002, 2005, 2007, 2008, and 2018). The CTD sections provide high-resolution data (1m in the vertical, and 5 to 10 km in the horizontal) of salinity and temperature. A monthly climatology of salinity based on the CTD dataset is used complementary to the mooring dataset, to provide an estimate of the undersampled near-surface salinity in the absence of Ice-

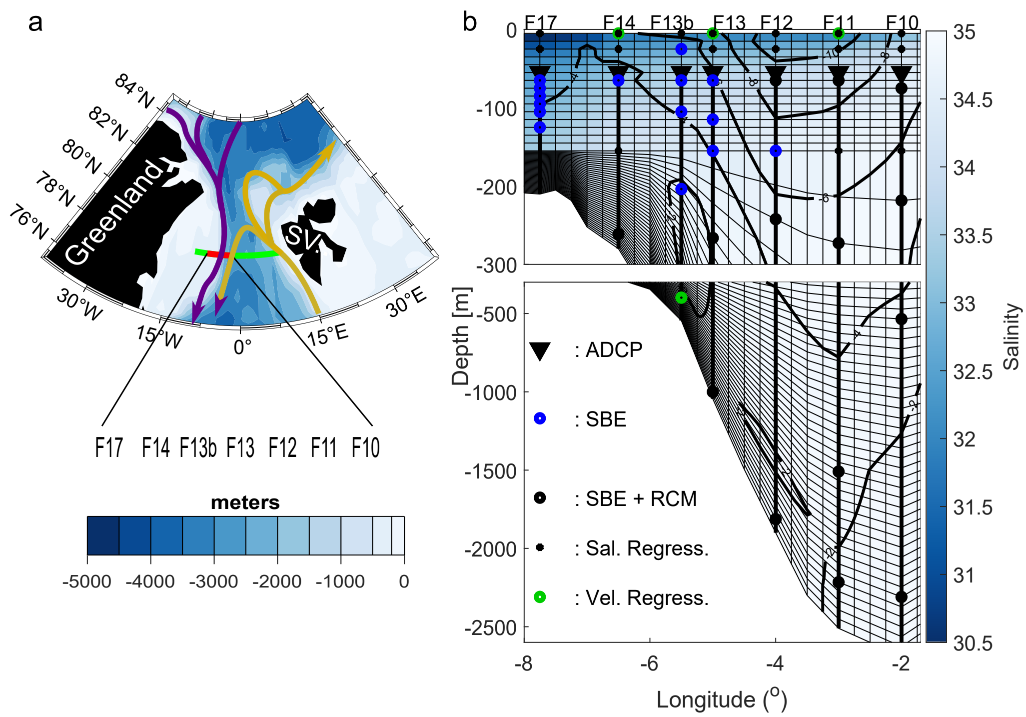

Figure 1. a) Map of the Fram Strait. The red line indicates the mooring array of the Fram Strait Outflow Observatory (FSAOO), and the green line the annually repeated CTD section. The magenta and yellow arrows indicate the pathways of East Greenland Current (EGC) the and West Spitsbergen Current (WSC) respectively. b) Setup of instruments in the FSAOO between September 2015 and August 2016. The colour shading and the black contours show the 2003-2009 mean salinity and velocity from the moorings. The mesh shows the interpolation grid and the dots the interpolant positions. The big black dots show positions of combined velocity (RCM) and salinity-temperature sensors (SBE), the blue dots positions of salinity-temperature sensors, the black triangles upward-looking Doppler velocity profilers (ADCP), the green dots the positions of velocity regression, and the small black dots the positions of salinity regression.

CATs, and to improve interpolation bias in the absence of instruments at $\sim$ 155 m. This climatology consists of the September and May data, which are interpolated cubically to provide a first order estimate of the seasonal cycle. For years with no May observations the long-term mean May value is used.

2.3 Gridding of data

For the calculation of transport through the array, we interpolate the monthly averaged velocity and salinity data on a grid with 0.25° horizontal resolution ($\sim$ 5.3 km). Moreover, to capture better the field over the steep continental slope, we use a bottom following grid below 155 m, and thus vertical resolution varies in space (Figure 1b) (De Steur et al., 2014). However, in case of data-gaps due to the lack or loss of instrumentation, and to limit interpolation bias and avoid extrapolation, estimations of monthly averaged salinity and velocity need to be added at essential positions in the cross-section. For velocity, this is done with linear regression from nearby instruments, with coefficients from other years' deployments, while salinity gaps are filled with linear regression from nearby instruments, with coefficients from the CTD climatology. Remaining gaps are filled

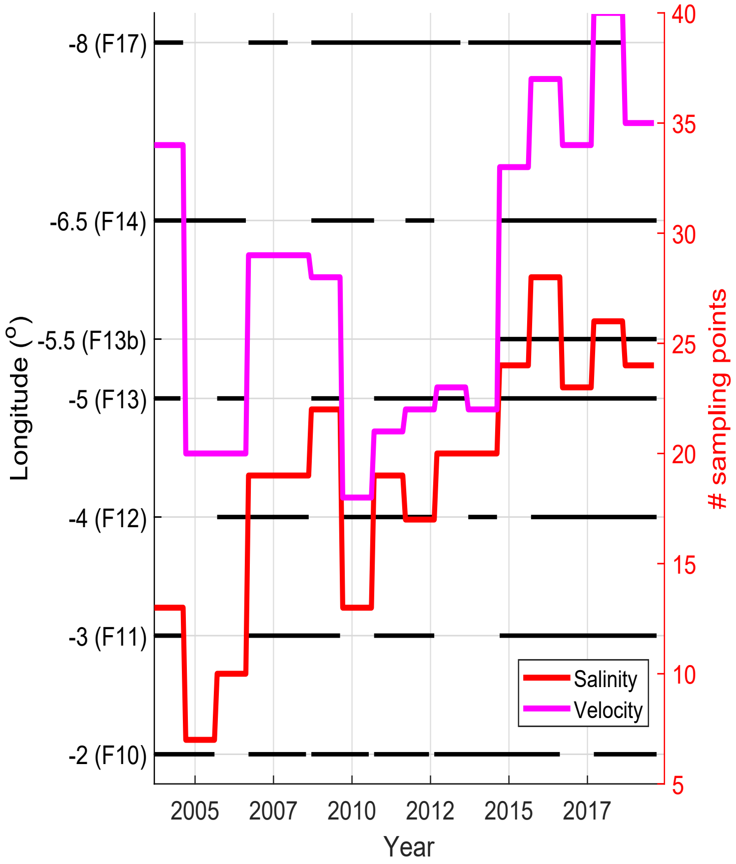

Figure 2. Sampling point number of the FSAOO for salinity and velocity per year-deployment (right axis). The horizontal black lines indicate the deployment period for each mooring (left axis).

with the long term mean for both variables (see text S1 of supporting information). Then, the monthly averaged velocity is linearly interpolated on the grid and mooring salinity is cubically interpolated in the vertical and linearly interpolated in the horizontal. Finally, the gridded salinity data are combined with temperature data (that followed the same process) to obtain density, and salinity is checked against and corrected for any density instabilities.

2.4 Methods

As of September 2013, the novel instruments provide year-round observations of salinity at 25 m (IceCATs) and 155 m (SBE37), improving our understanding of near-surface salinity seasonality, and stratification. Since September 2014, the newly deployed mooring F13b provide data at 5.5^oW, near the western edge of the core of the EGC. However, it is unclear how the previous transport estimates, when those instruments where not deployed, compare to those from recent years. To account for that, we exclude those three datasets, and in their absence calculate the offset of salinity and/or velocity. Then, we correct the previous estimates for the calculated offsets, and recalculate the FWT (Section 3.1).

We address the spatial and temporal variability of the EGC by comparing the mean gridded salinity and velocity fields for three averaging periods: period 1 between Sept. 2003 and Aug. 2009 showing relatively stable FWT from the EGC (De Steur et al., 2009); period 2 between Sept. 2009 and Aug. 2015 showing occurrences of increased FWT (De Steur et al., 2018) and period 3, after Aug. 2015, for which we present the updates of FWT. We examine the changes in salinity stratification with the salinity difference between 55 m and 155 m, as well as the changes in the extent of the Polar layer across the EGC (Section 3.2).

The freshwater and salt transports are determined as:

$$FWT_{(t)} = \int_{L_0}^{L_1} \int_{Z_0}^{Z_1} V_{(t,x,z)} \frac{S_r - S_{(t,x,z)}}{S_r} dzdx, \tag{1}$$

$$ST_{(t)} = \int_{L_0}^{L_1} \int_{Z_0}^{Z_1} V_{(t,x,z)} S_{(t,x,z)} \rho_{(t,x,z)} dzdx, \tag{2}$$

with $V_{(t,x,z)}$ and $S_{(t,x,z)}$ the velocity and salinity, and $\rho_{(t,x,z)}$ the density calculated from salinity and temperature. We set the reference salinity S_r to 34.9, the mean salinity of the Nordic Seas (Holfort & Meincke, 2005), but FWT is provided between brackets as well for $S_r = 34.8$, the mean salinity of the central Arctic Ocean (Aagaard & Carmack, 1989). In the horizontal, we integrate between F10 ($L_o = 2^oW$) and F17 ($L_1 = 8^oW$) while in the vertical we distinguish two cases: 1) Integration across the full vertical section ($Z_0 = 0$, $Z_1 = Z_{bottom}$), and 2) integration across the Polar Water (PW), here defined as the waters with negative temperature ($T < 0^oC$) and potential density anomaly (σ_θ) less than 27.7 kg/m^3 (Rudels et al., 2005) ($Z_o = 0$, $Z_1 = Z|_{PW depth}$) (Section 3.3).

The uncertainty in the calculation of FWT originates from the limited spatial coverage of the mooring array. More specifically, there are two types of uncertainty: The uncertainty of the interpolants and the uncertainty of gridding. The first refers to the uncertainty of the estimated values of velocity and salinity before gridding. This includes the sampling uncertainty of the instruments, the regression uncertainty from nearby instruments and the uncertainty of gap-filling with the long-term mean (see text S1 of supporting information). The second refers to the uncertainty of interpolating between a limited number of interpolants (Figure 1b), thus lacking details of the spatial variability. To estimate the uncertainty of gridding we use the mean section of the September CTD-dataset as the baseline, we sub-sample the salinity and geostrophic velocity sections at the interpolant positions, re-grid, and calculate the approximated FWT. Then, we use the absolute difference from the FWT of the baseline as the uncertainty. To include the uncertainty of the interpolants we allow random deviations from the baseline values, with the maximum deviation depending on the interpolant category and of its position in the section (see text S1 of supporting information), then calculate five hundred ensembles of the approximated FWT, and define the root-mean-square difference from the baseline value as the uncertainty (Section 3.4).

3 Results

3.1 Novel Data

The CTD climatology provides a first estimate of the seasonal cycle of salinity. Resulting from cubic interpolation between monthly averages from early September and May, it disregards any variability on shorter time scales. The salinity difference between 25 and 55 m observed by the year-round IceCAT deployments (ΔS_{obs}) shows some clear differences from the one estimated by the CTD climatology (ΔS_{ctd}), as it experiences abrupt changes within short periods (Figure 3). More specifically, in late September to early October, i.e. after the annually repeated CTD section, ΔS_{obs} increases as much

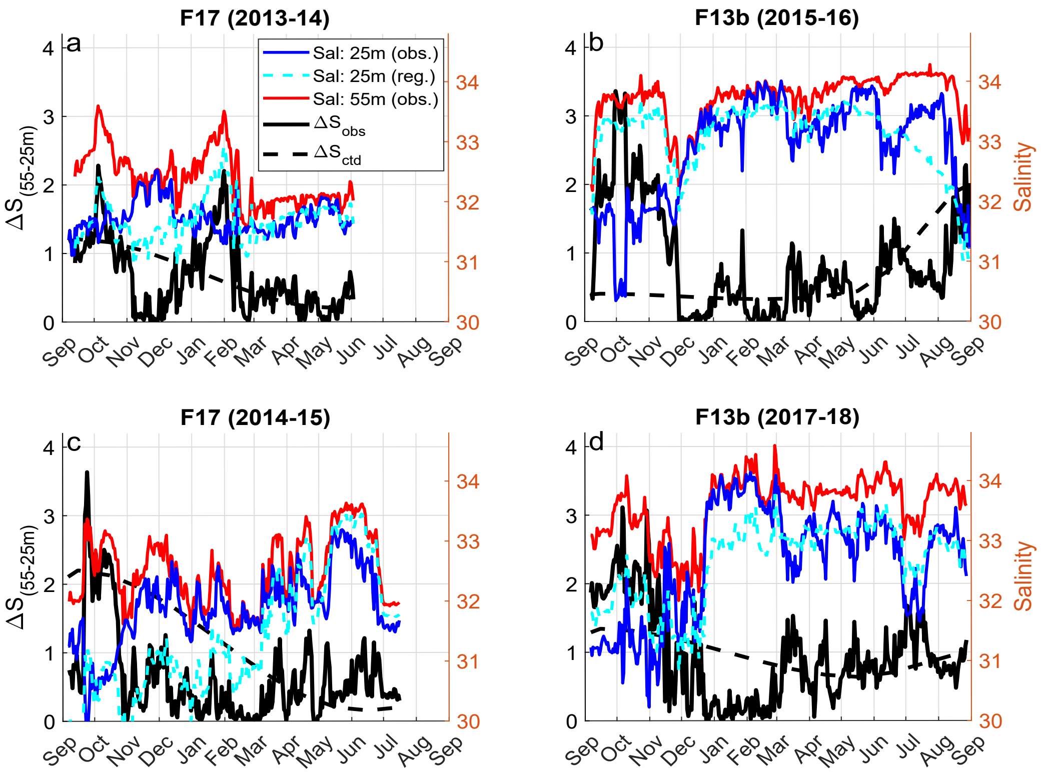

Figure 3. Observed and regressed daily means of salinity at 25 m from the four IceCAT deployments, and salinity at 55 m from the same mooring and year (right axis). Together, the observed salinity difference between 25 and 55 m (ΔS_{obs}) and the one calculated from the CTD climatology (ΔS_{CTD}) (left axis).

as 1.3 psu/day reaching the maximum stratification in October, which is not resolved by ΔS_{ctd}. In the core of the EGC at mooring F13b (Figure 3b, d), ΔS_{obs} experiences a sharp decrease in November - December due to a loss of summer stratification, mixing, and brine rejection, and remains well mixed up to late February - early March. On the shelf at mooring F17 (Figure 3a, c), ΔS_{obs} indicates well-mixed conditions in November and February in both deployments, while December and January differ between the two deployment years.

The differences between ΔS_{obs} and ΔS_{ctd} result in an offset between the observed (IceCATs) and regressed salinity at 25 m (Figure 3), and thus between the respective freshwater transports (FWT). Similarly, we calculate the offset related with the newly introduced mooring F13b at 5.5^oW (Sept. 2014), and with the SBE37 sensors deployed at $\sim$ 155 m (After Sept. 2013). Then, in the absence of these novel data, we correct the time series for those offsets. The correction of the time series is described in more detail in text S2 of the supporting information.

Seasonally averaged between Sept. 2003 - Sept. 2013, when no novel data where available, the correction results in a small decrease of the mean FWT by 0.8 mSV (Figure 4a), as the different offsets (varying from -6 mSV to +9 mSV) compensate each other (Figure 4b). More specifically, the SBE37 sensors introduced at 155 m result in a mean increase of 0.5 mSV by better resolving salinity in the lower halocline, and the mooring F13b at 5.5^oW to a mean decrease of -1.5 mSV by limiting interpolation errors at the western boundary of the EGC in summer and autumn (Figure 4b). Finally, the mean

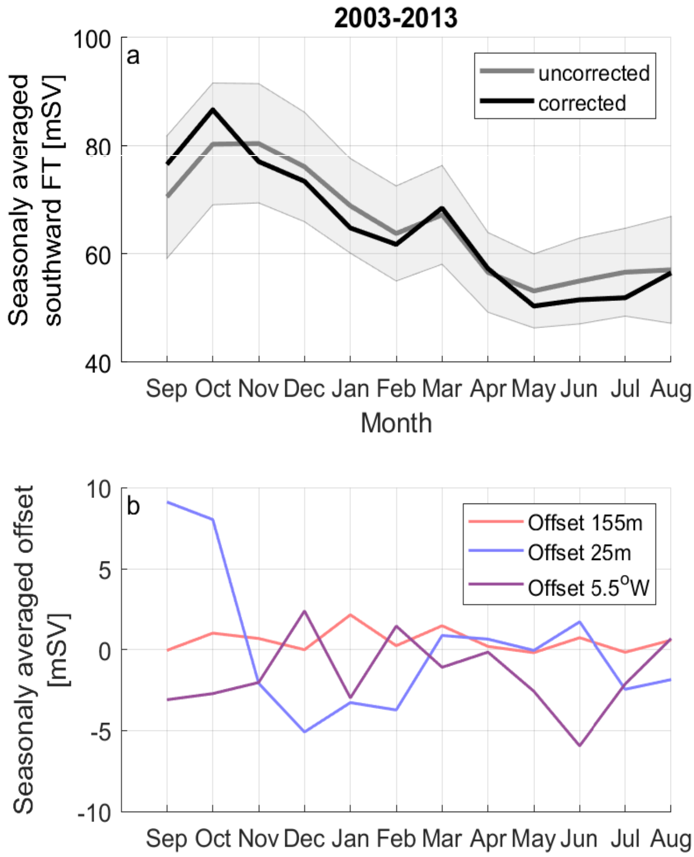

Figure 4. a) Southward FWT, seasonally averaged between 2003 and 2013, before and after the correction based on the novel data. The envelope shows the seasonally averaged uncertainty of FWT for the same period. b) Contributions of the three different novel datasets (IceCATs at 25 m, SBE37 at 155 m, mooring F13b at 5.5^oW) to the total offset.

offset from the IceCATs deployed at 25 m, and the corrections based on these data (see text S2 of supporting information) is small, however, with significant seasonal variation. The September and October FWT increases (9 mSV), reflecting the high stratification and low salinity observed at F13b (Figure 3b,d), but decreases between November and February (4 mSV), reflecting the well-mixed and more saline conditions in winter. Overall, the corrected time series remain within the uncertainty limits (Section 3.4) of the earlier estimates, implying that the time series of FWT in the EGC are not impacted significantly by the changing composition of the FSAOO array.

3.2 Hydrography and current velocity

Here, to allow comparison with earlier years, we present the corrected salinity and velocity data and analyse them for the three periods defined in Section 2 (period 1: Sept. 2003 - Aug. 2009, period 2: Sept. 2009 - Aug. 2015, period 3: Sept. 2015 - Aug. 2019). A test case where the novel instruments were excluded was tested and showed similar results. The mooring domain extends across the continental slope of Greenland between 8^oW and 2^oW, covering the deep western Fram Strait and a part of the shelf (8^oW-

6^oW). Close to the surface, two water masses are present. To the west, the southward moving buoyant Polar Waters (PW) with $T < 0^oC$ and potential density anomaly (σ_θ) smaller than 27.7 kg/m^3, and to the east and beneath the PW, the denser recirculating Atlantic Water (AW) (Figure 5a). The properties and position of the two water masses result in a tilt of the isopycnals and in a southward baroclinic velocity component that adds to the barotropic flow. Those two watermasses form the EGC with its core between 5^oW and 2^oW (Figure 5d).

Figure 5b and c show the salinity anomaly (ΔS) in periods 2 and 3 relative to period 1. In period 2 the fresh near-surface water (σ_θ <= 26.5 kg/m^3) became fresher (Figure 5b), while the layer below experienced only small changes. In period 3, the top layer remains fresher than in period 1 (Figure 5c), but the denser PW of the lower halocline experiences a significant increase in salinity. The freshening in the upper ocean is maximum in November-December, followed by September-October and is minimum in May-July where it is limited to the shelf. Salinification below the 26.5 kg/m^3 isopycnal occurs does not show a seasonal pattern (results not shown). This salinification is accompanied by an increase in temperature of the deeper PW shown by the upward and westward shift of the $T = 0^oC$ isothermal, which here defines the limit between PW and AW (Figure 5c). This shrinking of the PW domain is associated with increased presence of AW on the section. The data do not support an intensified recirculation of AW at this latitude, as the zonal component of the velocity shows a weaker westward flow during period 3 (Figure 6b), however, increased recirculation of AW could have occurred upstream of our array.

Figure 5d to f show the meridional velocity averaged over the three periods, and the anomaly of the two latter periods relative to period 1 is shown with contours (Figure 5e, f). In period 2, an additional shallow current core is observed over the shelf. This shelf current transports fresh PW southwards, contributing to the increased FWT observed over that period (De Steur et al., 2018). In period 3, the shelf current weakens, and only a narrow belt over the slope (centered at 5°W) on the western limit of the EGC maintains higher velocity compared to period 1, while the deeper core of the EGC east of 4°W weakens significantly. Overall, in period 3 the EGC appears weaker than period 1 and 2, but wider than period 1.

Southward velocity averaged over the top 155 m increased from 0.07 in period 1 to 0.08 m/s in period 2, while in period 3 it decreased to 0.06 m/s, though showing increased seasonality (Figure 6a). Similarly, salinity increases in period 3, as the salinification of the lower halocline exceeds the freshening of the top layer (Figure 6c). This salinification in the halocline results in shallower isopycnal depth (e.i. $\sigma_\theta = 27.7$ kg/m^3). This is less prominent at the eastern part of the domain (4^oW to 2^oW) (Figure 6d), resulting in a relaxation of the isopycnal tilt. This suggests that the observed weakening of the EGC is related partly to a decrease of its baroclinic component. From the September CTD data we calculate the baroclinic component of the flow (Figure 6a), exclude September 2014 which deviated more than three standard deviation from the mean, and find it to amount to 47% of the observed (mooring) velocity in September months, while 65% of the observed velocity decrease between periods 2 and 3 is explained by the reduction of the baroclinic component (seen in the CTD sections).

The changes in the spatial distribution of salinity in the western Fram Strait show increasing stratification in the PW, and a decreased depth and eastward extent of the PW domain related to increased presence of AW. Firstly, we present the changing salinity stratification of the PW with the mean salinity difference between 55 and 155 m (ΔS_{55-155}), averaged over the shelf from 8^oW to 6^oW (Figure 6e). Between period 1 and 2, ΔS_{55-155} increased from 1.2 to 1.4 psu, following the freshening at 55 m depth, and in period 3 it continued increasing reaching 1.6 psu, this time due to the salinification at 155 m. We note the difference of the shelf with the eastern part of the domain, where salinity stratification does not change significantly (Figure 6f), as salinity is increasing both at 55 and

Table 1. The long-term mean values (Sept. 2003 - Aug. 2019) and the means over the three averaging periods for the southward freshwater, salt and volume transport, and the freshwater content, integrated in the full section and the PW. The freshwater transport and content are calculated with respect to the reference salinity $S_r = 34.9$ [34.8]. The long-term means are given as well for the domain with $S < S_{ref}$, as used in De Steur et al. (2018).

Domain	Period	Southward Freshwater transp. [mSV]	Southward Salt transp. [kT/s]	Southward Volume transp. [SV]	Freshwater cont. [km^2]
Total	2003-2019	65.6 [43.8]	267.1	7.6	0.81 [0.34]
	1) 2003-2009	59.1 [35.8]	286.1	8.16	0.80 [0.32]
	2) 2009-2015	77.8 [57.1]	253.5	7.26	0.87 [0.39]
	3) 2015-2019	56.9 [35.9]	258.5	7.38	0.76 [0.28]
Polar	2003-2019	66.1 [62]	49.6	1.47	0.83 [0.78]
	1) 2003-2009	61.7 [57.7]	49.1	1.45	0.85 [0.79]
	2) 2009-2015	76.9 [72.3]	56.2	1.67	0.87 [0.8]
	3) 2015-2019	56.3 [52.9]	40.4	1.2	0.76 [0.7]
$S < S_{ref}$	2003-2019	70.17 [63.6]	124.4 [66]	3.6 [1.9]	0.92 [0.81]

155 m due to higher presence of AW over the whole depth. Finally, we quantify the retreat of the PW layer with the PW depth (Figure 6g), defined as the lower limit of the Polar layer averaged between 8^oW and 6^oW, and the PW distance (Figure 6h), indicating the distance of the PW-AW front (i.e. the 0^oC isotherm) at the surface from 6^oW. Both these variables experience a significant decrease in period 3: PW depth decreases from 182 m in period 2 to 157 m in period 3, while PW distance retreats from 71 km in period 2 to 61 km in period 3.

3.3 Transport of freshwater and salt

Here, we present the monthly mean time series of transport (Figure 7) for the two areas of integration, i.e. 1. the full vertical section and 2. PW only, both corrected for the introduction of novel instruments. The southward transport from the EGC is defined as positive. Along with the freshwater transport (FWT) (Figure 7a and b) and salt transport (ST) (Figure 7c and d, red line), we show the volume transport (VT) (Figure 7c and d, grey line) and freshwater content (FWC) (Figure 7e and f). FWT and FWC are calculated with respect to reference salinity $S_{ref} = 34.9$ and their values are provided with respect to $S_{ref} = 34.8$ as well between brackets.

A Reynolds decomposition of the FWT through the full section (Figure 7a) shows that the velocity anomaly contributes on average 63% [59%], and the FWC anomaly 33% [37%] to the FWT anomaly, while 4% [4%] is the contribution of the cross term anomaly. The ST time series coincides with that of the VT (Figure 7c, d), as the velocity anomaly contributes 99.94% to the ST anomaly. For the case of the EGC, and in a fixed boundary domain, the ST variability is defined by velocity only, as the velocity anomaly dominates over the salinity (and density) anomaly. However, in a domain with a (non-fixed) variable boundary, as is the PW layer ($\sigma_\theta < 27.7\ kg/m^3$ & $T < 0^oC$), part of the variability of VT and ST is explained by the variability of the boundary. Then, the VT and ST in the Polar layer (Figure 7d) is a function of velocity and of the area occupied by the PW. Those two contribute 84% [85%] and 16% [15%], respectively. The time series of FWT and ST anomaly, and the contribution from the different anomaly terms are shown in Figure S4 of Supplementary Information.

Due to their definition, FWC and FWT are larger when integrated up to $S = S_{ref}$ (table 1), as any salinity higher than the reference results in negative contribution to FWC and FWT. In the western Fram Strait, the FWT and FWC are controlled by processes within the Polar layer which accounts for 95% of the FWT and FWC occurring above the isohaline of $S = S_{ref}$ (table 1). More specifically, the increase of the FWT of the EGC in period 2 (Figure 7a, b), identified by De Steur et al. (2018), followed an increase of the VT and FWC in the PW (Figure 7d, f) due to increased-southward velocity (Figure 6a), and freshening of the top layer (Figure 5b), respectively. In period 3, FWT decreased as a result of lower VT and FWC in the PW, which followed the decreased southward velocity of the EGC and the salinification at the lower halocline (Figure 5c, f).

Focusing on the PW domain, a decrease of FWC and VT in June 2016 led to the second lowest FWT (18.37 [16.9] mSV) observed at the time since September 2004 (6.68 [6.14] mSV). Despite a general reduction in FWT in period 3, in 2017 between January - April and November - December, two strong FWT events (114 [108] mSV, 122 [117] mSV) occurred due to the concurring high FWC and VT. In June 2019, a very low FWT (14.41 mSV) was observed following mostly a large decrease of the VT. The apparent increased seasonal variability of velocity in period 3 (Figure 6a) contributes to an increase of the FWT variability, as two of the three lower FWT events of the whole record (June 2016, June 2019) have been observed in period 3, as well as two of the five higher (January - April, November - December 2017). Overall, since 2015, following the changes in the hydrography and current velocity in the western Fram Strait, the FWT of the EGC shows a marked change from before, not only in terms of a decrease in the average FWT, but in terms of increased variability as well.

3.4 Uncertainty analysis

Before September 2014, the significant data gaps (i.e. lost moorings and instrument failures) especially for the near surface velocity, resulted in high uncertainty that could reach up to 30% (Figure 8a, b). In Figure 8b we show the relative uncertainty time series, while the horizontal lines show the mooring deployments with at least one velocity sampling point above 100m. In the absence of velocity instruments in the upper 100m of the moorings F13 and F14, the uncertainty is higher than 20% for a large period of the year. After September 2014, when the new mooring F13b is included and more instruments are in place (i.e. new ADCPs at the surface and more instruments in the halocline), the uncertainty drops to below 10% and remains low in the absence of major instrumentation loss, for example the loss of F17 between Sept. 2018 - Sept. 2019.

The total uncertainty is largely defined by the uncertainty of gridding. For an estimate of this uncertainty, a single baseline dataset (mean of September CTD data) is used for all months (see Section 2.4), thus the seasonality of the gridding uncertainty is not addressed. The seasonality in the total uncertainty originates from the uncertainty at the interpolants (see text S1 of supporting information). Interpolants with data gaps are filled with the long term mean, or regressed with coefficients from other year deployments (see Section 2.3). Those methods are more precarious for August-September as in those months salinity and velocity are more variable from year to year, resulting to larger uncertainty (Figure 8c). Overall, the uncertainty of FWT is largely dependent on the availability of velocity instruments near the surface. This as upper ocean velocity is much more variable than salinity in time and space, resulting to high uncertainty when velocity data gaps are regressed or interpolated. We mention that the estimated interpolation uncertainty is dependent on the selection of the baseline dataset. In this analysis the mean September CTD dataset was used as a baseline, however, a sensitivity analysis with alternative baseline datasets, e.g. high-resolution model output, could give additional information.

4 Discussion

Since period 1, the salinity stratification within the Polar Water in the western Fram Strait has increased (Figure 6e). This is caused by freshening near the surface where $\sigma_\theta < 26.5\ kg/m^3$, and salinification in the layer $26.5 > \sigma_\theta > 27.7\ kg/m^3$ (Figure 5b, c). In addition, the Polar layer has thinned substantially in particular over the shelf since approximately mid-2014 (Figure 6g). This freshening and increasing stratification in the western Fram Strait is coherent with a shrinking ice-cover in the central Arctic Ocean which results in additional freshwater input at the surface through increased melt of sea ice during summer (Onarheim et al., 2018). The increasing salinity in the halocline could be due to enhanced winter-ice formation and brine rejection on the Arctic shelves. However, since it is associated with a shoaling of the 0°C isotherm at the same time, this indicates that the observed weakening of the cold halocline and shoaling of the Atlantic Water in the Eurasian Arctic (Polyakov et al., 2020) is emerging in the Fram Strait. Our observations demonstrate a so-called "Atlantification" in the western Fram Strait as described for the Barents Sea and Eurasian Basin (Polyakov et al., 2017; Lind et al., 2018; Polyakov et al., 2020). Additionally, the PW has retreated towards the shelf break notably in June 2015 (Figure 6h). We find that in recent years, signatures from upstream processes as well as locally driven changes have emerged in the Arctic outflow in the western Fram Strait. The cause of the distinct westward move of the PW-AW front in 2015, however, is subject of ongoing research.

The cumulated southward FWT anomaly with respect to its long-term mean (2003-2019) is shown in Figure 9 together with the FWC in the Beaufort Gyre (BG) obtained from Proshutinsky et al. (2019), both for a reference salinity of 34.8. This comparison shows that FW volume anomaly through Fram Strait, more or less, anticorrelates with the FWC in the BG. Between 2003-2009 (period 1), the FWC of the BG increased while the FWT in the Fram Strait was less than the mean. This coincided with an intensification of the BG (McPhee et al., 2009; Proshutinsky et al., 2009) and a diversion of riverine water from the Siberian shelves to the BG (Morison et al., 2012), that decreased the transport toward Fram Strait. Between 2009-2015 (period 2), the FWC increase stabilised during a temporary relaxation of the BG, and an eastward expansion of dynamic ocean topography (De Steur et al., 2013) allowed some freshwater from the BG to move toward Fram Strait leading to increased FWT. After 2015 (period 3), the FWC of the BG increased again and the FWT in the Fram Strait generally decreased. We do note, however, a significant FWT event was seen in the Fram Strait in winter 2017, which happened in concert with a temporary collapse of the BG and a reversal of surface circulation in the western Arctic in that year (Moore et al., 2018).

The availability of freshwater that converges in the BG during periods of intensification, and reduces the FWC in the Fram Strait suggests a clear link between the FWC of the BG and the FWT in the Fram Strait. However, the changes in the FWT of the Fram Strait between the three periods relate mostly to changing volume transport of the PW, and less to changing FWC (Figure 7b, d, and f). Further work is needed on identifying the possible links and driving mechanisms between the FWC of the BG and the FWT in the Fram Strait. This may include possible teleconnections between the sea-level pressure over the BG driving the storage of freshwater, and the wind forcing over the Fram Strait largely controlling the outflow (De Steur et al., 2018), sensitivity experiments with circulation models, as well as analysis of the Arctic dynamic topography over the Fram Strait.

After 2015, the southward velocity of the EGC decreased, partly as a result of a reduced baroclinic component. The decrease was most prominent in the core of the EGC (2°W - 4°W), in addition the southward current core seen over the shelf between 2009-2015 is not clearly observed after 2015. However, a portion of FWT on the shelf transported with this core may instead have occurred further west on the shelf, and may not have been captured by the moorings. This unknown shelf transport provides, at present, the largest uncertainty in our total FWT estimate at this latitude and enhanced monitoring of the shelf current system is required.

Finally, we presented the ST of the EGC which is independent of any reference value, addressing the ambiguity of FWC and FWT that depend on a reference salinity (Schauer & Losch, 2019). We found that in the EGC, the ST anomaly is not sensitive to salinity changes, as it is fully determined by the anomaly of velocity. This makes salt transport not suitable to identify salinity variations in the outflow. The independence of ST anomaly on salinity relates to the small value of a typical anomaly-to-mean ratio for salinity compared to velocity. Even though the FWT has limitations, it is still an efficient way to quantify and visualise changes in the combined salinity and velocity field and its effects on basin-scale hydrography. This, as the reference salinity in the nominator of the freshwater fraction (Equation 1) decreases the mean value of salinity without decreasing its anomaly from the mean, resulting in a comparable anomaly-to-mean ratio for velocity and freshwater fraction. However, we acknowledge that the use of different reference salinities when quantifying FWT and FWC in the literature leads to confusion. We suggest that if ST is preferred, it should be looked at in specific salinity domains, then ST anomaly depends on velocity directly, and on salinity through the limits of integration (Equation 2), without using a reference salinity.

5 Conclusions

Between 2015 and 2019, the freshwater transport (FWT) from the East Greenland Current (EGC) decreased due to reduced volume transport (VT) and freshwater content (FWC) in the Polar Water (PW: $\sigma_\theta < 27.7\ kg/m^3$ & $T < 0^oC$), which constitutes 95% of the FWT above the reference level of 34.9. From Sept. 2015 to Aug. 2019, the FWT of the PW reached an average of 56.3 (±4.5) mSV, 15% less than the long term mean. The salt transport (ST) anomaly coincides with the VT anomaly, meaning that ST is not sensitive to salinity changes. The average salt transport integrated over the full section between 2015-2019, was 258.5 kT/s of which the 40.4 kT/s occurred within the PW layer. Since 2015, both the VT and FWC in the PW experienced a significant decrease. The decreased FWC is related with a strong salinification of the lower halocline ($26.5 < \sigma_\theta < 27.7\ kg/m^3$) which counterbalances the freshening of the top layer ($\sigma_\theta < 26.5\ kg/m^3$). Between 2003-2019, the results show significant increase in the salinity stratification of the PW, as the salinity difference between 155 and 55 m increased by 0.63 psu, approximately 46 m thinning of the PW layer over the shelf, as well as a decreasing eastward extent of the PW from the shelf break. The salinification in the lower halocline is stronger over the shelf leading to a smaller tilt of the isopycnals and a weaker southward baroclinic component of the geostrophic velocity, which explained 65% of the mean-velocity reduction after 2015.

The long-term mean FWT of the EGC, observed with the mooring array, appears not very sensitive in changes of the array's composition. This means that estimates from previous years with less moored instruments are comparable with recent ones when coverage was higher. However, the newly deployed instruments demonstrated a seasonal bias in the earlier estimates. Salinity sensors (IceCATs) deployed at 25 m depth demonstrate that the FWT is in fact higher during September and October, and lower between November-February compared to the earlier applied estimates. Velocity sensors from the additional mooring F13B at 5.5^oW show that FWT is smaller in summer, however, the differences are not significant within the uncertainty of the earlier estimations. Nevertheless, the improved instrument coverage of the mooring array results in lower uncertainty in the calculation of FWT. The mean uncertainty after 2015 is 8%, significantly smaller than the mean uncertainty of previous years (17%).

Acknowledgments

This work was carried out in the FreshArc project supported by the Norwegian Research Council through the FRIPRO program (grant 286971). We like to thank Kristen Fossan for servicing the moorings and instruments and thanks to all crew of R/V Lance and R/V Kronprins Haakon. We thank Paul A. Dodd for providing processed CTD data. Finally, we thank Zoe Koenig for the insightful discussions on the uncertainty analysis. The data are available at https://data.npolar.no/dataset/8bb85388-327e-4b01-892c-5d1836d44ca4, and https://data.npolar.no/dataset/c4d80b64-25f6-4afd-b392-696430c3fd14.

References

Aagaard, K., & Carmack, E. (1968a). The East Greenland Current north of Denmark Strait: Part1. *Arctic*, *21*, 181-200.

Aagaard, K., & Carmack, E. C. (1989). The role of sea ice and other fresh water in the Arctic circulation. *Journal of Geophysical Research: Oceans*, *94*(C10), 14485-14498. Retrieved from `https://agupubs.onlinelibrary.wiley.com/doi/abs/10.1029/JC094iC10p14485` doi: https://doi.org/10.1029/JC094iC10p14485

Collins, M., Knutti, R., Arblaster, J., Dufresne, J.-L., Fichefet, T., Friedlingstein, P., ... Wehner, M. (2013). Chapter 12 - Long-term climate change: Projections, commitments and irreversibility. In IPCC (Ed.), *Climate change 2013: The physical science basis. ipcc working group i contribution to ar5.* Cambridge: Cambridge University Press. Retrieved from `http://pure.iiasa.ac.at/id/eprint/10551/`

Curry, B., Lee, C. M., Petrie, B., Moritz, R. E., & Kwok, R. (2014). Multiyear Volume, Liquid Freshwater, and Sea Ice Transports through Davis Strait, 2004–10. *Journal of Physical Oceanography*, *44*(4), 1244 - 1266. Retrieved from `https://journals.ametsoc.org/view/journals/phoc/44/4/jpo-d-13-0177.1.xml` doi: 10.1175/JPO-D-13-0177.1

De Steur, L., Hansen, E., Mauritzen, C., Beszczynska-Möller, A., & Fahrbach, E. (2014). Impact of recirculation on the East Greenland Current in Fram Strait: Results from moored current meter measurements between 1997 and 2009. *Deep Sea Research Part I: Oceanographic Research Papers*, *92*, 26-40. Retrieved from `https://www.sciencedirect.com/science/article/pii/S0967063714001009` doi: https://doi.org/10.1016/j.dsr.2014.05.018

De Steur, L., Hansen, E., Gerdes, R., Karcher, M., Fahrbach, E., & Holfort, J. (2009). Freshwater fluxes in the East Greenland Current: A decade of observations. *Geophysical Research Letters*, *36*(23). Retrieved from `https://agupubs.onlinelibrary.wiley.com/doi/abs/10.1029/2009GL041278` doi: 10.1029/2009GL041278

De Steur, L., Peralta-Ferriz, C., & Pavlova, O. (2018). Freshwater Export in the East Greenland Current Freshens the North Atlantic. *Geophysical Research Letters*, *45*(24), 13,359-13,366. Retrieved from `https://agupubs.onlinelibrary.wiley.com/doi/abs/10.1029/2018GL080207` doi: 10.1029/2018GL080207

De Steur, L., Steele, M., Hansen, E., Morison, J., Polyakov, I., Olsen, S. M., ... Schlosser, P. (2013). Hydrographic changes in the Lincoln Sea in the Arctic Ocean with focus on an upper ocean freshwater anomaly between 2007 and 2010. *Journal of Geophysical Research: Oceans*, *118*(9), 4699-4715. Retrieved from `https://agupubs.onlinelibrary.wiley.com/doi/abs/10.1002/jgrc.20341` doi: https://doi.org/10.1002/jgrc.20341

Giles, K., Laxon, S., & Ridout, A. e. a. (2012). Western Arctic Ocean freshwater storage increased by wind-driven spin-up of the Beaufort Gyre. *Nature Geosci*, *5*, 194-197. Retrieved from `https://doi.org/10.1038/ngeo1379`

Graham, R. M., Cohen, L., Petty, A. A., Boisvert, L. N., Rinke, A., Hudson, S. R., ... Granskog, M. A. (2017). Increasing frequency and duration of Arctic winter warming events. *Geophysical Research Letters*, *44*(13), 6974-6983. Retrieved from https://agupubs.onlinelibrary.wiley.com/doi/abs/10.1002/2017GL073395 doi: https://doi.org/10.1002/2017GL073395

Haine, T. W. N. (2020). Arctic Ocean Freshening Linked to Anthropogenic Climate Change: All Hands on Deck. *Geophysical Research Letters*, *47*(22), e2020GL090678. Retrieved from https://agupubs.onlinelibrary.wiley.com/doi/abs/10.1029/2020GL090678 (e2020GL090678 10.1029/2020GL090678) doi: https://doi.org/10.1029/2020GL090678

Haine, T. W. N., Curry, B., Gerdes, R., Hansen, E., Karcher, M., Lee, C., ... Woodgate, R. (2015). Arctic freshwater export: Status, mechanisms, and prospects. *Global and Planetary Change*, *125*, 13 - 35. Retrieved from http://www.sciencedirect.com/science/article/pii/S0921818114003129 doi: https://doi.org/10.1016/j.gloplacha.2014.11.013

Heuzé, C. (2017). North Atlantic deep water formation and AMOC in CMIP5 models. *Ocean Science*, *13*(4), 609–622. Retrieved from https://os.copernicus.org/articles/13/609/2017/ doi: 10.5194/os-13-609-2017

Holfort, J., & Meincke, J. (2005, 12). Time series of freshwater-transport on the East Greenland Shelf at 74N. *Meteorologische Zeitschrift*, *14*(6), 703-710. Retrieved from http://dx.doi.org/10.1127/0941-2948/2005/0079 doi: 10.1127/0941-2948/2005/0079

Jahn, A., & Laiho, R. (2020). Forced Changes in the Arctic Freshwater Budget Emerge in the Early 21st Century. *Geophysical Research Letters*, *47*(15), e2020GL088854. Retrieved from https://agupubs.onlinelibrary.wiley.com/doi/abs/10.1029/2020GL088854 (e2020GL088854 10.1029/2020GL088854) doi: https://doi.org/10.1029/2020GL088854

Le Bras, I., Straneo, F., Muilwijk, M., Smedsrud, L. H., Li, F., Lozier, M. S., & Holliday, N. P. (2021). How Much Arctic Fresh Water Participates in the Subpolar Overturning Circulation? *Journal of Physical Oceanography*, *51*(3), 955 - 973. Retrieved from https://journals.ametsoc.org/view/journals/phoc/51/3/JPO-D-20-0240.1.xml doi: 10.1175/JPO-D-20-0240.1

Lind, S., Ingvaldsen, R., & Furevik, T. (2018). Arctic warming hotspot in the northern Barents Sea linked to declining sea-ice import. *Nature Clim Change*, *8*, 634–639. Retrieved from https://doi.org/10.1038/s41558-018-0205-y

Lique, C., Holland, M. M., Dibike, Y. B., Lawrence, D. M., & Screen, J. A. (2016). Modeling the Arctic freshwater system and its integration in the global system: Lessons learned and future challenges. *Journal of Geophysical Research: Biogeosciences*, *121*(3), 540-566. Retrieved from https://agupubs.onlinelibrary.wiley.com/doi/abs/10.1002/2015JG003120 doi: https://doi.org/10.1002/2015JG003120

Lobelle, D., Beaulieu, C., Livina, V., Sévellec, F., & Frajka-Williams, E. (2020). Detectability of an AMOC Decline in Current and Projected Climate Changes. *Geophysical Research Letters*, *47*(20), e2020GL089974. Retrieved from https://agupubs.onlinelibrary.wiley.com/doi/abs/10.1029/2020GL089974 (e2020GL089974 10.1029/2020GL089974) doi: https://doi.org/10.1029/2020GL089974

Marnela, M., Rudels, B., Goszczko, I., Beszczynska-Möller, A., & Schauer, U. (2016). Fram Strait and Greenland Sea transports, water masses, and water mass transformations 1999–2010 (and beyond). *Journal of Geophysical Research: Oceans*, *121*(4), 2314-2346. Retrieved from https://agupubs.onlinelibrary.wiley.com/doi/abs/10.1002/2015JC011312 doi: https://doi.org/10.1002/2015JC011312

McPhee, M. G., Proshutinsky, A., Morison, J. H., Steele, M., & Alkire, M. B. (2009). Rapid change in freshwater content of the Arctic Ocean. *Geophysical Research Letters*, *36*(10). Retrieved from https://agupubs.onlinelibrary.wiley.com/doi/abs/10.1029/2009GL037525 doi: https://doi.org/10.1029/

2009GL037525

Moore, G. W. K., Schweiger, A., Zhang, J., & Steele, M. (2018). Collapse of the 2017 Winter Beaufort High: A Response to Thinning Sea Ice? *Geophysical Research Letters*, *45*(6), 2860-2869. Retrieved from https://agupubs.onlinelibrary.wiley.com/doi/abs/10.1002/2017GL076446 doi: https://doi.org/10.1002/2017GL076446

Morison, J., Kwok, R., Peralta-Ferriz, C., Alkire, M., Rigor, I., Andersen, R., & Steele, M. (2012). Changing Arctic Ocean freshwater pathways. *Journal of Geophysical Research: Oceans*, *481*(70). Retrieved from https://doi.org/10.1038/nature10705 doi: 10.1038/nature10705

Mosby, H. (1962). Water, salt, and heat balance of the Polar Ocean, with special emphasis on the Fram Strait. *Norsk Polarinst. Skr*, *188*, 1-53.

Onarheim, I. H., Eldevik, T., Smedsrud, L. H., & Stroeve, J. C. (2018). Seasonal and Regional Manifestation of Arctic Sea Ice Loss. *Journal of Climate*, *31*(12), 4917 - 4932. Retrieved from https://journals.ametsoc.org/view/journals/clim/31/12/jcli-d-17-0427.1.xml doi: 10.1175/JCLI-D-17-0427.1

Polyakov, I., Pnyushkov, A., Alkire, M., Ashik, I., Baumann, T., Carmack, E., ... A., Y. (2017). Greater role for Atlantic inflows on sea-ice loss in the Eurasian Basin of the Arctic Ocean. *Science.*, *356*, 285-291. doi: 10.1126/science.aai8204

Polyakov, I., Rippeth, T. P., Fer, I., Alkire, M. B., Baumann, T. M., Carmack, E. C., ... Rember, R. (2020). Weakening of Cold Halocline Layer Exposes Sea Ice to Oceanic Heat in the Eastern Arctic Ocean. *Journal of Climate*, *33*(18), 8107 - 8123. Retrieved from https://journals.ametsoc.org/view/journals/clim/33/18/jcliD190976.xml doi: 10.1175/JCLI-D-19-0976.1

Proshutinsky, A., Krishfield, R., Timmermans, M.-L., Toole, J., Carmack, E., McLaughlin, F., ... Shimada, K. (2009). Beaufort Gyre freshwater reservoir: State and variability from observations. *Journal of Geophysical Research: Oceans*, *114*(C1). Retrieved from https://agupubs.onlinelibrary.wiley.com/doi/abs/10.1029/2008JC005104 doi: 10.1029/2008JC005104

Proshutinsky, A., Krishfield, R., Toole, J. M., Timmermans, M.-L., Williams, W., Zimmermann, S., ... Zhao, J. (2019). Analysis of the Beaufort Gyre Freshwater Content in 2003–2018. *Journal of Geophysical Research: Oceans*, *124*(12), 9658-9689. Retrieved from https://agupubs.onlinelibrary.wiley.com/doi/abs/10.1029/2019JC015281 doi: https://doi.org/10.1029/2019JC015281

Quadfasel, D., Gascard, J.-C., & Koltermann, K.-P. (1987). Large-scale oceanography in Fram Strait during the 1984 Marginal Ice Zone Experiment. *Journal of Geophysical Research: Oceans*, *92*(C7), 6719-6728. Retrieved from https://agupubs.onlinelibrary.wiley.com/doi/abs/10.1029/JC092iC07p06719 doi: https://doi.org/10.1029/JC092iC07p06719

Rabe, B., Dodd, P. A., Hansen, E., Falck, E., Schauer, U., Mackensen, A., ... Cox, K. (2013). Liquid export of Arctic freshwater components through the Fram Strait 1998-2011. *Ocean Science*, *9*(1), 91-109. Retrieved from https://os.copernicus.org/articles/9/91/2013/ doi: 10.5194/os-9-91-2013

Rabe, B., Karcher, M., Kauker, F., Schauer, U., Toole, J. M., Krishfield, R. A., ... Su, J. (2014). Arctic Ocean basin liquid freshwater storage trend 1992–2012. *Geophysical Research Letters*, *41*(3), 961-968. Retrieved from https://agupubs.onlinelibrary.wiley.com/doi/abs/10.1002/2013GL058121 doi: 10.1002/2013GL058121

Rudels, B., Björk, G., Nilsson, J., Winsor, P., Lake, I., & Nohr, C. (2005). The interaction between waters from the Arctic Ocean and the Nordic Seas north of Fram Strait and along the East Greenland Current: results from the Arctic Ocean-02 Oden expedition. *Journal of Marine Systems*, *55*(1), 1-30. Retrieved from https://www.sciencedirect.com/science/article/pii/S0924796304002015 doi: https://doi.org/10.1016/j.jmarsys.2004.06.008

Schauer, U., & Losch, M. (2019, 08). "Freshwater" in the Ocean is Not a Useful Parameter in Climate Research. *Journal of Physical Oceanography*, *49*(9), 2309-2321. Retrieved from `https://doi.org/10.1175/JPO-D-19-0102.1` doi: 10.1175/JPO-D-19-0102.1

Shu, Q., Qiao, F., Song, Z., Zhao, J., & Li, X. (2018). Projected Freshening of the Arctic Ocean in the 21st Century. *Journal of Geophysical Research: Oceans*, *123*(12), 9232-9244. Retrieved from `https://agupubs.onlinelibrary.wiley.com/doi/abs/10.1029/2018JC014036` doi: https://doi.org/10.1029/2018JC014036

Stommel, H. (1961). Thermohaline Convection with Two Stable Regimes of Flow. *Tellus*, *13*(2), 224-230. Retrieved from `https://doi.org/10.3402/tellusa.v13i2.9491` doi: 10.3402/tellusa.v13i2.9491

Zhang, J., Steele, M., Runciman, K., Dewey, S., Morison, J., Lee, C., ... Toole, J. (2016). The Beaufort Gyre intensification and stabilization: A model-observation synthesis. *Journal of Geophysical Research: Oceans*, *121*(11), 7933-7952. Retrieved from `https://agupubs.onlinelibrary.wiley.com/doi/abs/10.1002/2016JC012196` doi: https://doi.org/10.1002/2016JC012196

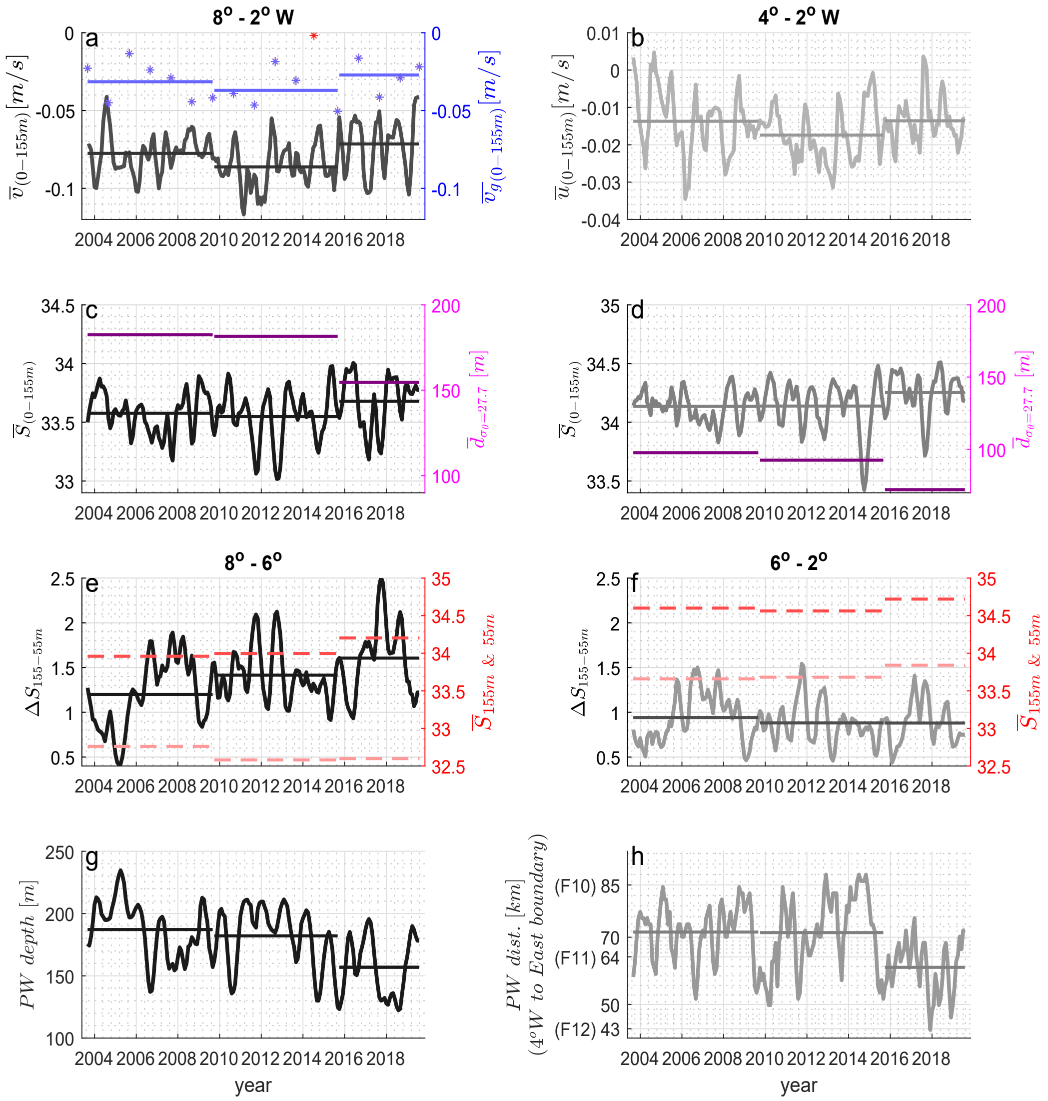

Figure 5. a) Mean salinity section over period 1, b-c) salinity anomaly of periods 2 and 3 relative to period 1. The solid contours indicate the mean position of the isopycnals $\sigma_\theta = 26.5$ kg/m^3, and $\sigma_\theta = 27.7$ kg/m^3, the isotherm $T = 0^oC$ and the isohaline $S = 34.9$ psu in each period. The dashed contours in b and c indicate the mean position of the isolines over period 1. d-f) Mean velocity section over the three periods. For period 2 and 3 the contours show the anomaly relative to period 1.

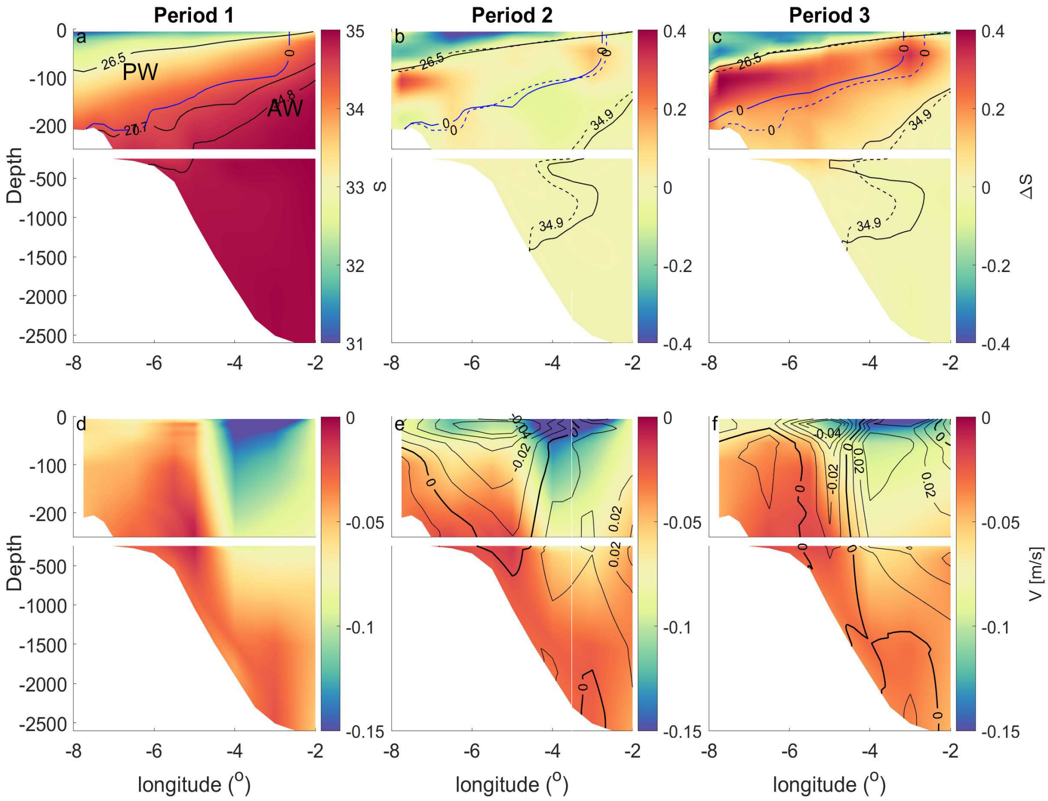

Figure 6. a-b) Mean meridional velocity between 8^o - 2^oW, and zonal velocity between 4^o - 2^oW averaged in the top 155 m. The baroclinic meridional component calculated from the Sept. CTD data is presented with the blue stars (the red star shows the anomalous month of Sept. 2014 which is excluded from the calculations). c-d) Mean salinity between 8^o - 2^oW, and between 4^o - 2^oW averaged in the top 155 m. The average depth of the σ_θ=27.7 kg/m^3 isopycnal is presented for the three periods with the magenta lines. e-f) Salinity difference between 55 and 155 m depth, averaged between 8^o - 6^oW and 6^o - 2^oW. The mean values of salinity at 55 and 155 m are shown with the red (155 m) and pale red (55 m) dashed lines. g) Polar Water depth defined as the lower limit of the Polar layer averaged between 8^o - 6^oW, and h) Polar Water distance defined as the surface distance of the PW-AW front (0°C isotherm) from 6^oW.

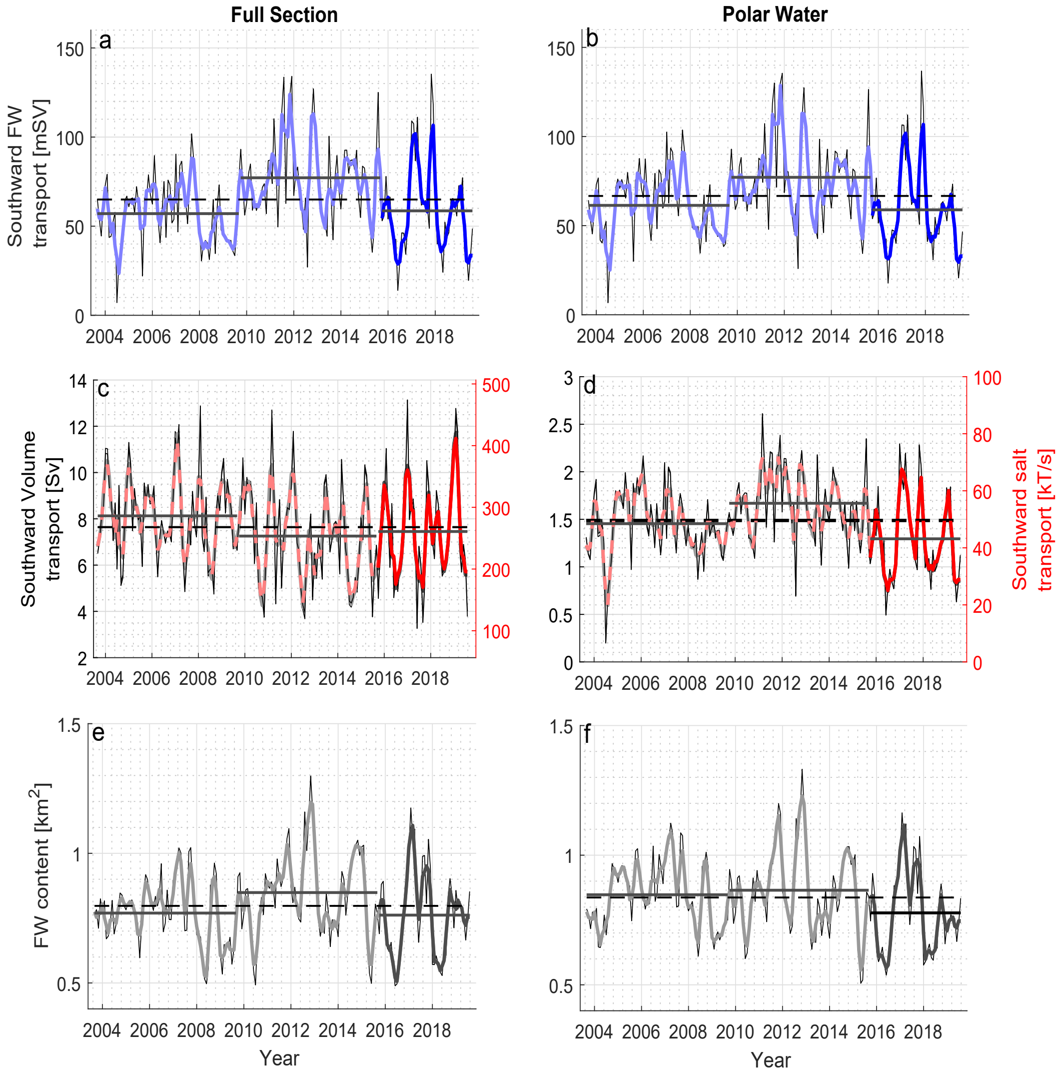

Figure 7. Time series of southward freshwater (a, b), salt and volume transport (c, d), and freshwater content (e, f) integrated in the full vertical section (left), and the Polar layer ($\sigma < 27.7$ kg/m^3, $T < 0^oC$) (right) . ($S_{ref} = 34.9$). The thin-black and thick-coloured time series indicate the monthly values and three-month running means, respectively. The horizontal lines indicate the long-term means (dashed: Sept. 2003 - Aug. 2019) and the means over the three averaging periods (solid: period 1: Sept. 2003 - Aug. 2009, period 2: Sept. 2009 - Aug. 2015, period 3: Sept. 2015 - Aug. 2019).

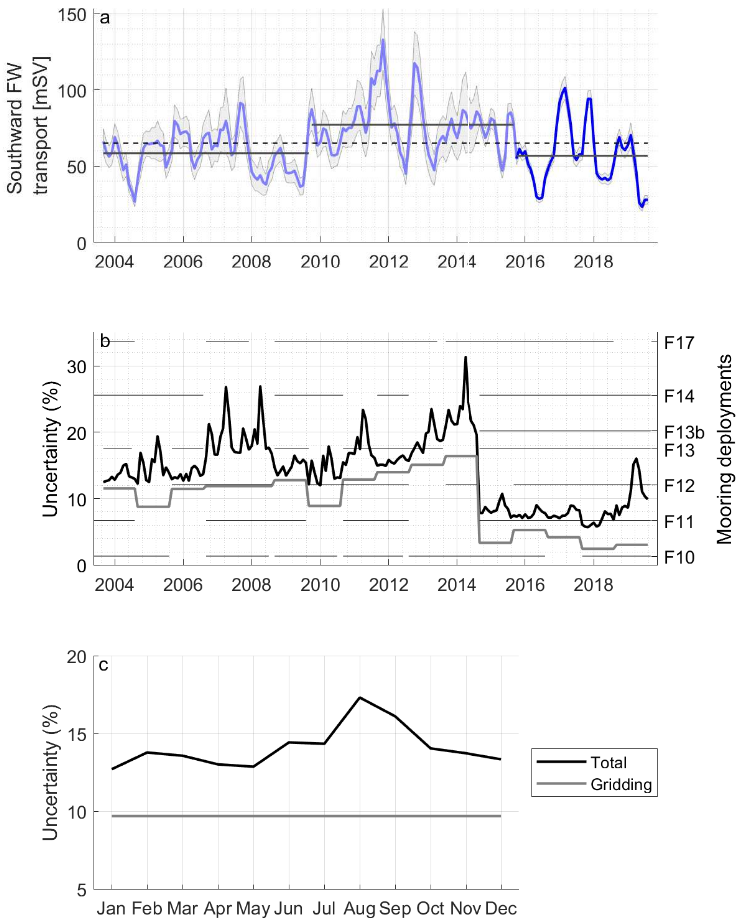

Figure 8. a) Time-series of freshwater transport with the respective uncertainty envelope. b) Relative uncertainty of the freshwater transport (left axis). The uncertainty of gridding is provided together with the total uncertainty which includes the uncertainty of the interpolants as well. The horizontal lines indicate the mooring deployments with at least one velocity sampling point above 100m depth (right axis). c) seasonally averaged uncertainty (2003-2019).

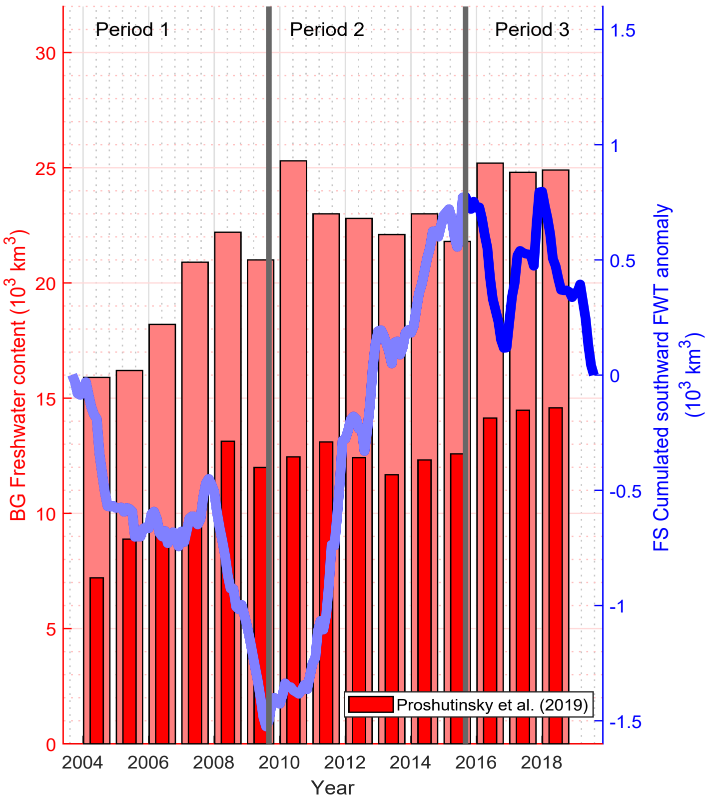

Figure 9. Cumulative southward FWT anomaly relative to 34.8 in the Fram Strait, with respect to the long term mean of 65.6 mSV between 2003-2019. Increasing (decreasing) values denote more (less) southward freshwater transport than 65.6 mSV. The blue and pale blue lines shows the time-series before and after September 2015. The red and pale red bars show the FWC in the Beaufort Gyre relative to 34.8 from moorings and ITP data presented in Proshutinsky et al. (2019).